



This is a repository copy of *Surface and sub-surface integrity of Ti-6Al-4V components produced by selective electron beam melting with post-build finish machining*.

White Rose Research Online URL for this paper:
<http://eprints.whiterose.ac.uk/162692/>

Version: Published Version

Proceedings Paper:

Childerhouse, T., Hernandez-Nava, E., M'Saoubi, R. et al. (2 more authors) (2020) Surface and sub-surface integrity of Ti-6Al-4V components produced by selective electron beam melting with post-build finish machining. In: Arrazola, P.J. and Madariaga, A., (eds.) *Procedia CIRP. 5th CIRP Conference on Surface Integrity (CSI 2020)*, 01-05 Jun 2020, Vitoria-Gasteiz, Basque Country, Spain. Elsevier BV , pp. 309-314.

<https://doi.org/10.1016/j.procir.2020.02.018>

Reuse

This article is distributed under the terms of the Creative Commons Attribution-NonCommercial-NoDerivs (CC BY-NC-ND) licence. This licence only allows you to download this work and share it with others as long as you credit the authors, but you can't change the article in any way or use it commercially. More information and the full terms of the licence here: <https://creativecommons.org/licenses/>

Takedown

If you consider content in White Rose Research Online to be in breach of UK law, please notify us by emailing eprints@whiterose.ac.uk including the URL of the record and the reason for the withdrawal request.



eprints@whiterose.ac.uk
<https://eprints.whiterose.ac.uk/>

5th CIRP CSI 2020

Surface and sub-surface integrity of Ti-6Al-4V components produced by selective electron beam melting with post-build finish machining

Thomas Childerhouse^{a*}, Everth Hernandez-Nava^a, Rachid M'Saoubi^b, Nikolaos Tapoglou^c,
Martin Jackson^a

^aDepartment of Materials Science and Engineering, The University of Sheffield, Sir Robert Hadfield Building, Mappin Street, Sheffield, S1 3JD, UK

^bMaterials & Technology Development, Seco Tools AB, SE73782, Fagersta, Sweden

^cAdvanced Manufacturing Research Centre with Boeing, University of Sheffield, Rotherham, S60 5TZ, UK

* Corresponding author. E-mail address: tchilderhouse1@sheffield.ac.uk

Abstract

The emergence of metal additive manufacturing (AM) processes offer manufacturers a promising alternative to traditional forging and casting techniques for the production of near net shape titanium alloy components. However, limitations in both the surface finish quality and the geometric accuracy of parts produced by AM means that post-build finish machining of the part remains to be a requirement to produce high precision components. Furthermore, the fatigue performance of material produced directly by these processes is often limited by both the poor surface finish and porosity related defects which occur within the material. This study investigates the implications of machining stock allowance on the surface integrity of Ti-6Al-4V specimens produced by selective electron beam melting (SEBM) followed by post-build finish machining. The study revealed that the exposure of porosity related defects on the newly machined surface varied depending on the depth of material removed from the as-built specimen surface during machining. Four point bend fatigue testing of the specimens was carried out to determine the effect of the exposed surface defects on the fatigue performance of the material. This study highlights that the non-uniform distribution of pores within SEBM Ti-6Al-4V means that careful considerations must be given regarding machining stock allowance in the design of these components due to the implications of material removal depth on surface integrity.

© 2020 The Authors. Published by Elsevier B.V.

This is an open access article under the CC BY-NC-ND license (<http://creativecommons.org/licenses/by-nc-nd/4.0/>)

Peer-review under responsibility of the scientific committee of the 5th CIRP CSI 2020

Keywords: Additive manufacturing; finish machining; low cycle fatigue

1. Introduction

The emergence of AM technologies which use a titanium alloy feedstock material offers manufacturers an alternative to traditional processes for the production of titanium alloy components. These technologies are capable at producing near net shape components and can therefore offer significant improvements in material utilisation and reduce machining costs compared to conventional process routes [1]. These economic benefits make AM a promising alternative to conventional processes, as their adoption could offer cost

savings for the aerospace industry and have the potential to make titanium use more economically viable for other industries. The suitability of AM for the manufacture of bespoke components is demonstrated by the medical industry who have adopted powder bed fusion type AM processes, such as SEBM, for the production of orthopedic implants [2, 3]. These applications showcase the capabilities of AM for the fabrication of highly complex geometries through the production of lattice type structures, which allow for better tissue in-growth and osseointegration compared to implants manufactured by traditional techniques. For the aerospace and

automotive industries, the potential for AM is demonstrated by the manufacture of a variety of demonstrator components [4, 5]. Regardless, these processes remain to be implemented commercially. This can be attributed to the limited and highly variable fatigue performance of material produced by AM [6]. In samples produced by SEBM, fatigue cracks have been found to initiate at stress concentration sites on the surface of the part. This occurs due to the rough surface finish of parts produced by this method [7]. However, polishing and/or finish machining has been shown to be an effective method at preventing fatigue failure from crack initiation at the part's surface and in polished/machined samples, fatigue failure has been found to occur due to crack nucleation at porosity related defects [8].

The SEBM process involves the consolidation of metal powder particles. This is carried out by the process of scanning an electron beam over a layer of deposited powder to form a melt pool, which then solidifies. This process is then repeated, one cross section layer at a time, until the final part is produced [9]. This beam scanning method typically involves two different melt strategies, referred to as *contouring* and *hatching*. The initial contouring strategy, involves scanning the beam around the perimeter of the cross-section to melt the boundary of the part. During contouring, a strategy known as *MultiBeam* is employed which rapidly moves the beam around the contouring path to achieve active melting at several different locations simultaneously. Following the contouring stage, hatching is carried out to melt the remaining powder and this involves melting within the contoured region by rastering the beam from side-to-side. The purpose of these melting strategies is to, improve the surface quality of the part when contouring by producing a shallow melt-pool and increasing the build rate during hatching by employing a more rapid beam speed [10].

The main concern for the use of SEBM components in applications where fatigue performance is critical, is the occurrence of porosity related defects [11]. Various pore morphologies have been observed in SEBM material and these are typically characterised as either irregularly shaped or spherical [12]. Irregularly shaped pores are often larger ($>100\mu\text{m}$) and are attributed to lack of fusion between powder particles due to insufficient melting. Spherical pores, which are typically smaller in size ($<100\mu\text{m}$), are attributed to residual argon gas entrapped within the powder feedstock during powder atomisation. The presence of porosity within titanium alloys produced by SEBM is influenced by a number of factors, most notably build parameters such as beam speed and current, which affect the melt pool size [13]. However, where these parameters are optimised, achieving fully-dense parts remains to be difficult without post-process treatments such as hot isostatic pressing (HIPing) [14].

In a study by Tammis-Williams et al. [15], analysis of Ti-6Al-4V samples using X-ray Computed Tomography (XCT), found that the spatial distribution of pores in material produced by SEBM is not random, rather it is influenced by the beam scanning strategy implemented by the machine manufacturer. The study revealed that, in samples produced using the machine manufacturers default melt strategy, the number density of pores within the contoured region ($<0.8\text{ mm}$ from the sample surface) was significantly less compared to that within the region of the material consolidated by the hatching strategy.

Furthermore, it was observed that spherical type pores contributed to the majority (97%) of the total pore volume fraction and these were found to be predominantly distributed within the hatched region. Irregularly shaped pores however, were found have a much smaller contribution to the overall volume fraction and were found to occur in both the contoured and hatched regions. Differences in the melt strategies used when either contouring or hatching was the suggested reason for the greater volume fraction of pores in the hatched region. This difference was attributed to the higher beam speeds used during hatching, which generate a smaller melt pool and in-turn offers less opportunity for gas entrapped within the powder feedstock to escape during processing. Moreover, the study observed a peak in porosity at 0.9 mm from the sample surface, corresponding with the position close to the final contouring beam path and the initial hatched path. The authors suggested that the occurrence of this peak was due to the dumping of pores pushed forward by the solidification front during contouring.

To improve the surface finish and fatigue performance of AM components, post-build finish machining can be carried out to remove the outer-skin of the part and generate a machined surface [16]. However, the non-uniform distribution of pores within SEBM material has the potential to have major implications on the exposure of porosity related defects following material removal. This study investigates the effects of finish machining depth on the surface condition of Ti-6Al-4V specimens produced by SEBM using standard Arcam build parameters. Specimens have been machined at two different depth levels to generate machined surfaces located in the region of the build produced by both the contouring and hatching strategies and porosity exposure on these newly generated surfaces is compared. Furthermore, fatigue performance has been shown to be effected by the location and morphology of porosity related defects within the material, with larger defects and defects closer to the surface being the most detrimental [17]. Therefore, this study employs fatigue testing using a four point bend test method to investigate the influence of porosity distribution on fatigue performance. Such as method has been also been demonstrated to show the effect of machining induced damage on fatigue in titanium alloys [18].

2. Experimental method

2.1. SEBM Build

The SEBM samples produced for this study were built using a feedstock material of Ti-6Al-4V pre-alloyed plasma atomized powder supplied by Arcam. The powder size distribution was reported by Arcam to range from 45 to 106 μm with an oxygen content of 0.150 wt. %. Specimen blanks of dimensions 5.3 x 20.6 x 120 mm were built using the Arcam Q20 system implementing control software version 5.2.52 at the University of Sheffield. The build process was carried out using a single sample orientation with the build direction depicted by the Z-direction in the schematic shown in Fig. 1a. All of the specimens used for this investigation were produced during a single build. Prior to commencing the build, the build chamber was taken below a 2×10^{-4} mBar vacuum to reduce the potential for oxidation of the material during processing.

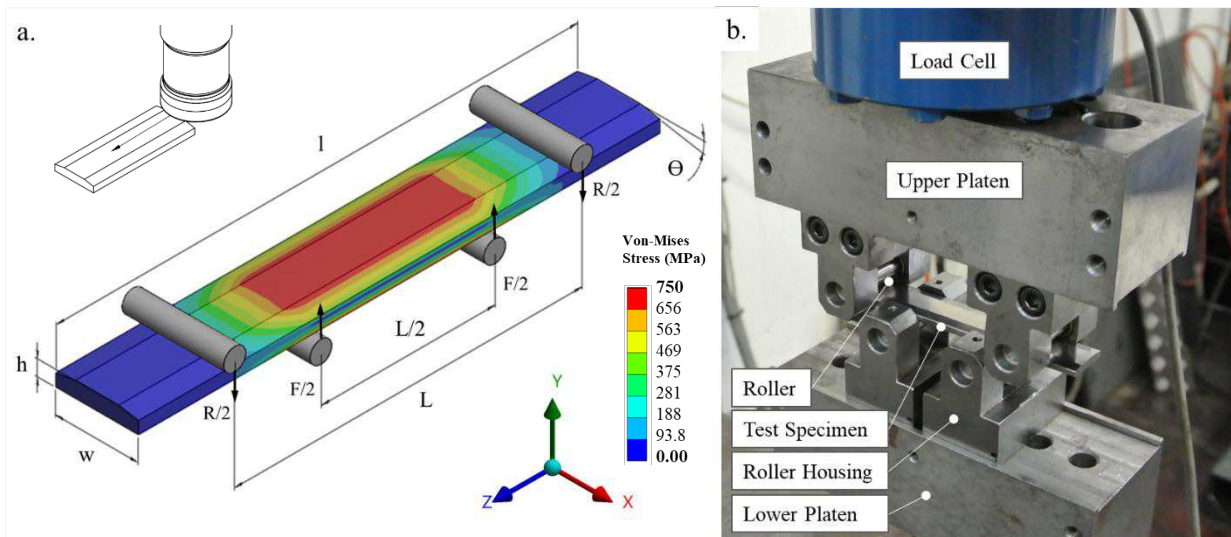


Fig. 1. Four point bend test method used to assess fatigue performance of the specimens: (a) Schematic representation of the test method and specimen geometry with superimposed FEA stress distribution. (b) Annotated photograph of the four point bend test rig at the University of Sheffield.

The process then involved initial pre-heating of the build plate to 500 °C with a de-focused beam spot with a focus offset of +60 mA. Following pre-heating of the build plate, a consecutive process of raking a layer of powder onto the plate, further pre-heating of the deposited powder layer using a de-focused beam and melting of the newly deposited powder layer using a sharper beam spot, with a focus offset of +45mA, was carried out. This process was then repeated until the build was completed. The standard layer thickness of 90 μm for the Q20 system was used throughout the build process.

The beam scanning method used for powder melting employed the standard Arcam strategy, consisting initially of contouring the outline of the cross-section, followed by melting within the contoured outline using a hatching strategy. The contouring stage involved two passes of the beam with a line offset of 0.27 mm. During contouring, the *MultiBeam* strategy was employed. The approximate contoured feature thickness for the part was 0.80 mm from the specimen surface. For the hatching stage, a continuous beam path following a raster type motion was used with a line offset of 0.18 mm. During melting, the beam speed was adapted according to Arcam's *AutoCalculation* compensations for the given beam current, which was setup with an 8.97 mA base setting.

2.2. Finish machining

Specimen blanks were machined to their final geometry at the University of Sheffield's Advanced Manufacturing Research Centre, using the DMG Mori DMU Evo-40 universal machining centre. Specimens were machined to respective dimensions of 3.6, 19.0, and 120 mm for height (h), width (w) and length (l) and featured a chamfer angle (Θ) of 10° (Fig. 1a). Machining this geometry from the SEBM specimen blanks involved holding the workpiece in four different orientations to remove the as-built surface from each of the faces in the Z-X and Z-Y planes (Fig. 1a). Material was removed by a face milling process with the tool feed direction indicated by the Z-direction in Fig. 1a. Tooling, provided by Seco Tools,

comprised of a square shoulder milling cutter (R217.94-2525.0-08-4A) of diameter 25 mm and PVD coated carbide F40M grade inserts (LOEX080408TR-M08) with a corner radius of 0.80 mm. During machining, Blaser Swisslube Vasco 7000 cutting fluid was supplied via through tool delivery.

The specimens were machined by removing material from the critical surface (the upwards facing surface in Fig. 1a) to depths of both 0.50 and 1.00 mm relative to the original as-built part surface. These depths were selected to represent typical stock allowance settings that could be included on components produced by powder bed AM processes, as well as on the basis that the newly generated surfaces would be located in the region of the part consolidated by both the contouring and hatching melt strategies. During machining, identical cutting parameters (as described in Table 1) were used. This was to ensure that, any differences in the integrity of the surfaces generated at the two different conditions could be attributed to the location of the newly generated surface in the as-built part, rather than any significant differences in cutting conditions. To achieve a material removal depth of 0.50 and 1.00 mm, both single and two pass processes were carried out with an axial depth of cut (a_p) of 0.50 mm. In addition to the two conditions described, specimens were also produced to a third condition, whereby the critical specimen surface was left in its as-built condition.

2.3. Fatigue testing

Conventional fatigue testing methods typically involve the testing of cylindrical specimens (usually machined by external turning) which are subject to axial loading conditions. However, for the purposes of this study, it was desirable to test specimens produced by a milling process. Fatigue testing was therefore carried out using a four point bend method using the test rig shown in in Fig. 1b. In this arrangement, dynamic loading was applied to the specimen and distributed through a pair of lower rollers, with the specimen supported by a pair of upper static rollers at a span distance, $L = 80$ mm. This test allowed for a large region of maximum tensile stress (shown by

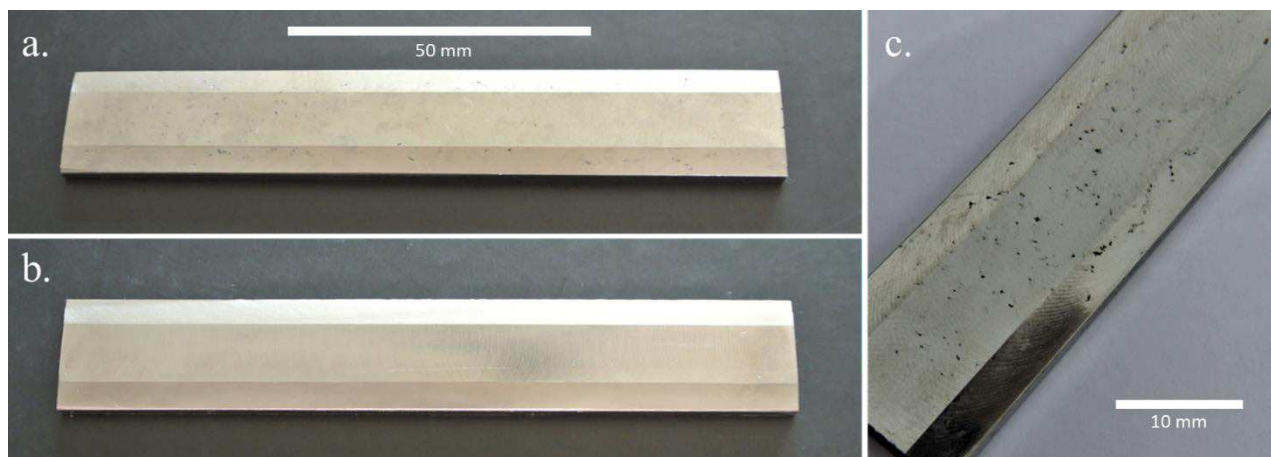


Fig. 2. Photographs of SEBM Ti-6Al-4V specimens following post-build finish machining to remove material to a depth level of: (a) 1.00 mm, (b) 0.50 mm from the as-built specimen surface, and (c) a close up image showing the severity of porosity exposure when a material removal depth of 1.00 mm is employed.

the FEA stress distribution in Fig. 1a) to be applied to the upwards facing surface of the specimen, which had been machined at the two depth levels investigated in this study.

Fatigue testing was carried out at ambient conditions using a Nene 12 kN servo-hydraulic test machine. This was controlled via a Moog Smartest One controller receiving feedback from a load cell mounted on the machine. Testing was carried out until the point of failure, with each specimen loaded under sinusoidal conditions at a frequency of 5 Hz. Specimens were subject to a stress ratio, $R = 0.1$ and a peak stress, $S_{Max} = 750$ MPa.

Table 1. Summary of post-build finish machining parameters.

Cutting parameter	Condition 1	Condition 2
Cutting speed, V_c (m/min)	48	48
Feed per tooth, f_c (mm/tooth)	0.15	0.15
Axial depth of cut, a_p (mm)	0.50	0.50
Number of passes in a_p	1	2

3. Results and discussion

Characterisation of the machined specimens revealed the presence of exposed defects at the newly machined surface when a total material removal depth of 1.00 mm was employed. Whereas the surface of specimens machined to a depth of 0.50 mm showed no such defects. Fig. 2 shows examples of specimens machined at the two conditions and highlights the significant amount of defects present on the specimen surface following machining to a depth of 1.00 mm. Confocal microscopy images of these defects (highlighted in Fig. 3b) show the presence of un-melted powder particles. This suggests that, these defects are lack of fusion defects [12] present in the as-built SEBM material which have been exposed at the surface during post-build machining.

The influence of material removal depth on defect exposure indicates that a similar spatial distribution of porosity related defects demonstrated by Tammam-Williams et al. [15], is also present in material produced by the Arcam Q20 system used in this study. It is notable that specimens produced in Tammam-Williams work were produced using an earlier anode-based Arcam S12 system, rather than the present cathode-based

system. The high level of porosity exposure observed on the surfaces machined below the 0.80 mm contoured feature depth is suggestive that, the hatching melt strategy is less effective than contouring at producing fully dense material. Furthermore, due to the significant number of defects which can be observed when machining to a depth of 1.00 mm, it appears that there is a high concentration of defects which occur at the interface between the material consolidated by the contouring and hatching melt strategies. It is possible that, the concentration of defects at this location may occur due to insufficient melting of the powder where the beam turns the corner at the end of each pass during hatching.

Characterisation of the specimen surface topography has been carried out using an Alicona SL InfiniteFocus confocal microscope. 3D surface roughness metrics for each of the surface conditions produced in the study are given in Table 2. The values quoted for the two machined conditions correspond with the respective surfaces shown in Figs. 3a and 3b. Porosity related defects exposed on the machined surface are highlighted in Fig. 3b. Three surface defects are visible, with the larger (~500 μm across) irregular shaped defect on the left of the image typical of that of a lack of fusion type defect. The two defects on the right of the image are smaller in size (~100 μm across) and it is possible that these features could both originate from the same lack of fusion defect, which was mostly removed during machining leaving these extremities. The 3D topography scan (Fig. 3c) shows the depth beneath the machined surface which the defects penetrate and indicates a maximum depth of 180 μm for the irregular shaped defect. Fig. 4 shows large area stitched 3D topography scans of the as-built and machined specimen surfaces. The rough surface finish of the material in its as-built condition is pictured showing a maximum relative peak height of ~280 μm . In Fig. 4b the significance of the number of defects present over a large area of the machined surface is shown. The 3D surface roughness metrics, presented in Table 2, highlight the improvements in surface finish of the machined specimens compared to those in the as-built condition. These metrics show the detrimental effects of defect exposure on surface finish when specimens are machined to a total depth of 1.00 mm, which is highlighted by the increased metrics for S_{sk} and S_{ku} , indicating the presence of cavities on the machined surface.

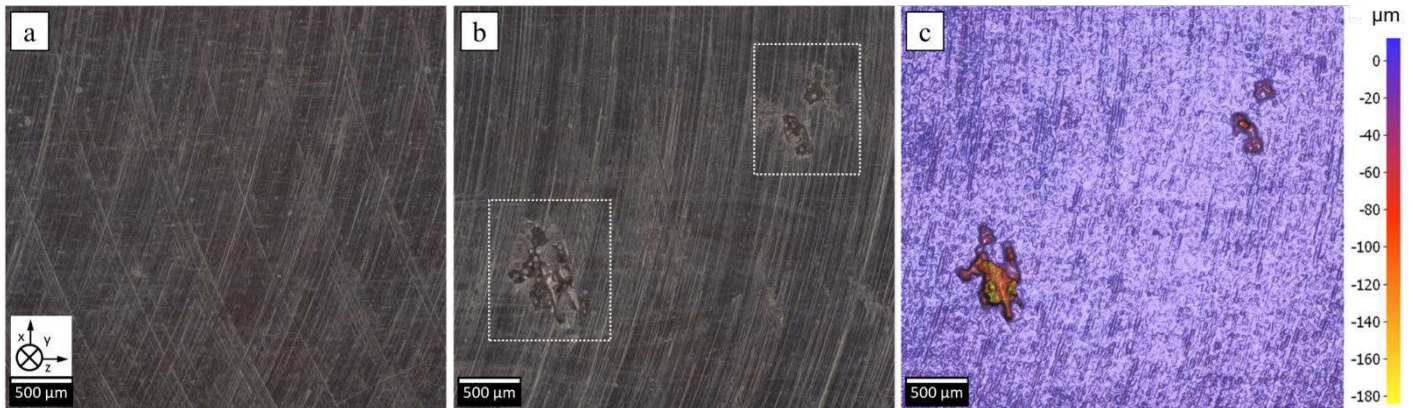


Fig. 3. Confocal microscopy images of the SEBM specimen surfaces following finish machining to remove material at depths of (a) 0.50 and (b) 1.00 mm relative to the original as-built specimen surface with exposed defects highlighted. (c) 3D topography scan when machining to remove material at a depth of 1.00 mm.

Table 2. Summary of 3D surface roughness metrics.

Surface Condition	Sa (μm)	Sq (μm)	Ssk	Sku
As-Built	40.01	50.20	-0.595	3.184
Machined – 0.50 mm	1.510	2.032	-0.237	5.686
Machined – 1.00 mm	2.637	10.13	-10.46	126.7

3.1. Fatigue test results

Four point bend fatigue testing was successfully carried out to the point of failure for each specimen. Three specimens of each condition were tested and the mean number of cycles to failure (N_f) as well as the standard deviation for each specimen condition are given in Table 3. For each specimen, the number of cycles to failure was recorded to be in the low cycle fatigue (LCF) range and failure of each specimen occurred in the region of maximum stress highlighted in Fig. 1a. Results indicated that, specimens which had not undergone any post-build finish machining of the critical specimen surface had the lowest fatigue performance. Specimens machined to a depth of 0.50 mm showed no significant performance improvement. However, specimens machined to a total depth of 1.00 mm showed a significant improvement in fatigue performance, achieving on average more than double the number of cycles before failure compared to those in the other two conditions. This finding was contrary to initial assumptions, as the specimens which showed the highest fatigue performance were

also those which were found to have exposed surface defects and a rougher surface profile. These defects were expected to have a significantly detrimental effect on fatigue performance due to their location in the maximum stress region of the specimen under the loads applied during testing. It is possible however, that when specimens were machined to a total depth of 1.00 mm, a significant volume of the high concentration of defects present at the interface of material consolidated by the hatching and contouring melt strategies were removed. This is based on the fact that, they were located within the layer of material removed during machining. The remaining defects, which were reduced in size, are therefore present mostly at the surface. In contrast, defects present in material where only a 0.50 mm depth of material was machined away, would remain mostly intact following machining. This is because, machining to this depth fails to reach the interface located approximately 0.80 mm beneath the as-built part surface. Assuming that the failure of the machined specimens is due to crack initiation at porosity related defects, this could explain the improved fatigue performance in specimens machined to a depth of 1.00 mm, as in these specimens, the total defect volume has been reduced and it could be possible that the stress concentration effect of the remaining surface/near-surface defects is less significant than that of the larger, intact subsurface defects present in the samples machined only to a depth of 0.50 mm.

Another possible reason for the improved fatigue performance in specimens where the 1.00 mm material removal depth has been employed, could be due to machining induced residual stresses. Assuming that a compressive to tensile

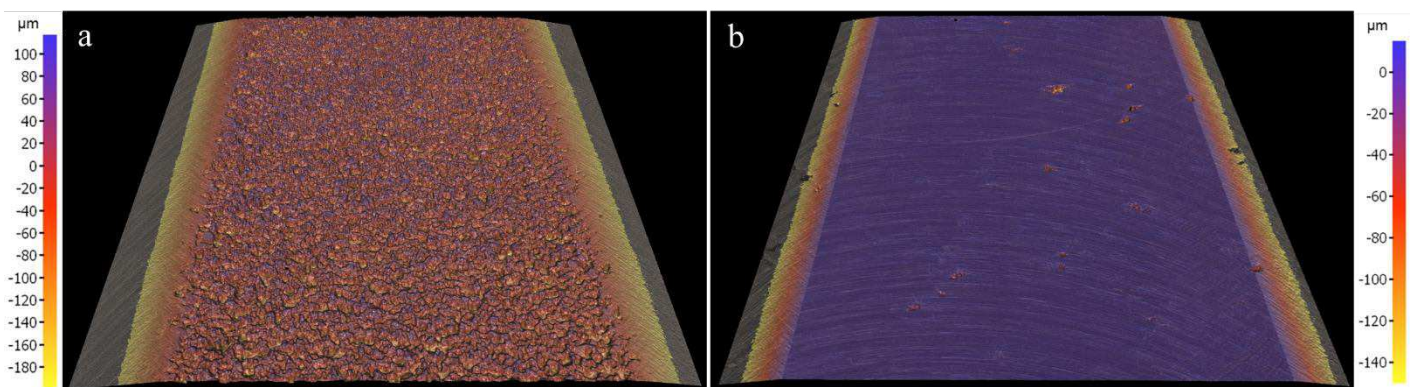


Fig. 4. 3D surface topography scans of SEBM specimens with the critical specimen surface in (a) the as-built condition and (b) following machining to remove material to a total depth of 1.00 mm relative to the as-built part surface.

residual stress profile from the specimen surface occurs, which is typically induced during face milling [19], it is possible that, the surface defects present in specimens machined to 1.00 mm are located within the region of maximum compressive residual stress. This would have an effect of an overall reduced tensile stress at the surface during testing, which would mean that these defects could have less of a detrimental effect than the subsurface defects present in specimens machined to a depth of 0.50 mm, which are predominantly located in a region where residual stresses are less compressive and the overall tensile stress is higher.

Table 3. Summary of four point bend fatigue test results at $S_{Max} = 750$ MPa

Specimen Condition	Mean Cycles, N_f	Standard Deviation (%)
SEBM As-Built	1351	29.7
SEBM Machined – 0.50 mm	1705	17.7
SEBM Machined – 1.00 mm	3446	4.8

4. Conclusions

This study has demonstrated that, post-build finish machining can be an effective technique for improving the surface finish and fatigue performance of SEBM Ti-6Al-4V components. Furthermore, it revealed that, due to the spatial distribution of porosity related defects within the as-built material, the depth of material removed during finish machining had significant implications on the surface integrity of the newly machined surface, due to the exposure of porosity related defects during machining. Surfaces of specimens which had been machined by to a total depth of 1.00 mm, relative to the as-built part surface, possessed a significant number of surface defects which were characterised to be lack of fusion defects and these were found to measure to up to 500 μm across and penetrate to a maximum depth of 180 μm . In contrast, specimens machined to a depth of only 0.50 mm were found to be free of such surface defects. Low cycle fatigue testing using a four point bend test method was carried out and revealed that, specimens machined to a depth of 1.00 mm performed significantly better than those which had not undergone any machining or had been machined to a depth of only 0.50 mm. These results suggest that it may be necessary to remove additional material from SEBM components during machining for the removal of defects concentrated in the sub-surface region of the part. This could potentially limit the material utilisation benefits offered by the process.

Acknowledgements

This study was funded by the EPSRC Industrial Doctorate Centre in Machining Science (EP/L016257/1) and MAPP the EPSRC Future Manufacturing Hub in Manufacture using Advanced Powder Processes (EP/P006566/1) as well as Seco Tools and Element Six. The authors would also like to acknowledge the Henry Royce Institute for Advanced Materials, funded through EPSRC grants EP/R00661X/1, EP/S019367/1, EP/P02470X/1 and EP/P025285/1, for the financial support and EBM-ARCAM Q20 access at Royce@Sheffield.

References

- [1] T. Childerhouse and M. Jackson, "Near Net Shape Manufacture of Titanium Alloy Components from Powder and Wire : A Review of State-of-the-Art Process Routes," *Metals*, vol. 9, no. 6, 2019.
- [2] V. V. Popov, J. Gary, M.-k. A. Kovalevsky, G. Dzhenezhera, E. Strokin, A. Kolomiets, J. Ramon, and G. Muller-kamskii, "Design and 3D-printing of titanium bone implants : brief review of approach and clinical cases," *Biomedical Engineering Letters*, vol. 8, no. 4, pp. 337–344, 2018.
- [3] W. Harun, N. Manam, M. Kamariah, S. Sharif, A. Zulkifly, I. Ahmad, and H. Miura, "A review of powdered additive manufacturing techniques for Ti-6Al-4V biomedical applications," *Powder Technology*, vol. 331, pp. 74–97, 2018.
- [4] F. Caiazzo, F. Cardaropoli, V. Alfieri, V. Sergi, and L. Cuccaro, "Experimental analysis of selective laser melting process for Ti-64 turbine blade manufacturing," *XIX International Symposium on High-Power Laser Systems and Applications*, no. January 2013, p. 86771H, 2013.
- [5] L. Nickels, "AM and aerospace : an ideal combination," *Metal Powder Report*, vol. 70, no. 6, pp. 300–303, 2015.
- [6] J. J. Lewandowski and M. Seifi, "Metal Additive Manufacturing: A Review of Mechanical Properties," *Annual Review of Materials Research*, vol. 46, no. 1, pp. 151–186, 2016.
- [7] K. S. Chan, M. Koike, R. L. Mason, and T. Okabe, "Fatigue Life of Titanium Alloys Fabricated by Additive Layer Manufacturing Techniques for Dental Implants," *Metallurgical and Materials Transactions A: Physical Metallurgy and Materials Science*, vol. 44A, pp. 1010–1022, 2013.
- [8] P. Edwards, A. O'Conner, and M. Ramulu, "Electron Beam Additive Manufacturing of Titanium Components : Properties and Performance," *Journal of Manufacturing Science and Engineering*, vol. 135, no. December 2013, pp. 1–7, 2013.
- [9] L.-c. Zhang, Y. Liu, S. Li, and Y. Hao, "Additive Manufacturing of Titanium Alloys by Electron Beam Melting : A Review," *Advanced Engineering Materials*, vol. 1700842, pp. 1–16, 2018.
- [10] E. Hernandez-Nava, C. Smith, F. Derguiti, S. Tammas-Williams, F. Leonard, P. J. Withers, I. Todd, and R. Goodall, "The effect of defects on the mechanical response of Ti-6Al-4V cubic lattice structures fabricated by electron beam melting" *Acta Materialia*, vol. 108, pp. 279–292, 2016.
- [11] S. Tammas-Williams, P. J. Withers, I. Todd, and P. B. Prangnell, "The Influence of Porosity on Fatigue Crack Initiation in Additively Manufactured Titanium Components," *Scientific Reports*, no. February 2016, pp. 1–13, 2017.
- [12] M. Qian, W. Xu, M. Brandt, and H. P. Tang, "Additive manufacturing and postprocessing of Ti-6Al-4V for superior mechanical properties," *MRS Bulletin*, vol. 41, no. 10, pp. 775–783, 2016.
- [13] R. Cunningham, S. P. Narra, T. Ozturk, J. Beuth, and A. D. Rollett, "Evaluating the Effect of Processing Parameters on Porosity in Electron Beam Melted Ti-6Al-4V via Synchrotron X-ray Microtomography," *JOM*, vol. 68, no. 3, pp. 765–771, 2016.
- [14] S. Tammas-Williams, P. J. Withers, I. Todd, and P. B. Prangnell, "The Effectiveness of Hot Isostatic Pressing for Closing Porosity in Selective Electron Beam Melting," *Metallurgical and Materials Transactions A*, vol. 47, no. 5, pp. 1939–1946, 2016.
- [15] S. Tammas-Williams, H. Zhao, F. L'eonard, F. Derguti, I. Todd, and P. B. Prangnell, "XCT analysis of the influence of melt strategies on defect population in Ti-6Al-4V components manufactured by Selective Electron Beam Melting," *Materials Characterization*, vol. 102, pp. 47–61, 2015.
- [16] H. Masuo, Y. Tanaka, S. Morokoshi, H. Yagura, T. Uchida, Y. Yamamoto, and Y. Marakami, "Effects of Defects , Surface Roughness and HIP on Fatigue Strength of Ti-6Al-4V manufactured by Additive Manufacturing," *3rd International Symposium on Fatigue Design and Material Defects*, 2017.
- [17] Y. Murakami, "Material defects as the basis of fatigue design," *International Journal of Fatigue*, vol. 41, pp. 2–10, 2012.
- [18] A. Cox, S. Herbert, J.-P. Villain-Chastre, S. Turner and M. Jackson, "The effect of machining and induced surface deformation on the fatigue performance of a high strength metastable β titanium alloy," *International Journal of Fatigue*, vol. 124, pp. 26–33, 2019.
- [19] J. Köhler, T. Grove, O. Maifß and B. Denkena, "Residual Stress in Milled Titanium Parts," *1st CIRP Global Web Conference on Interdisciplinary Research in Production Engineering*, 2012.